Biomass-Gas-and-Nuclear-To-Liquids (BGNTL) Processes Part I: Model Development and Simulation

J. Alexander Scott and Thomas A. Adams II *

Department of Chemical Engineering, McMaster University, 1280 Main St. West, Hamilton, ON, Canada

New polygeneration processes for the co-production of liquid fuels (Fischer-Tropsch liquids, methanol, and dimethyl ether) and electricity are presented. The processes use a combination of biomass, natural gas, and nuclear energy as primary energy feeds. Chemical process models were created and used to simulate candidate versions of the process, using combinations of models ranging from complex multi-scale models to standard process flowsheet models. The simulation results are presented for an Ontario, Canada case study to obtain key metrics such as efficiency and product conversions. Sample Aspen Plus files are provided in the supplementary material to be used by others.

Keywords: biomass, natural gas, nuclear energy, synthetic fuels, polygeneration

INTRODUCTION

The government of the province of Ontario, Canada, has made a commitment to decarbonizing its energy infrastructure.[1] For example, all bulk electricity production from coal in the province has ceased, and the Atikokan generating station was converted from a coal-fired to a wood-pellet-fired thermal power plant at 205 MW (the largest of its kind in North America).[2] Ontario also has a cap-and-trade style carbon market,[3] with the Federal government setting a carbon tax floor (which increases annually) in case the provincial system does not result in high enough carbon prices.[4] In addition, Ontario's electricity grid makes heavy use of nuclear, hydropower, and non-hydropower renewable resources (wind and solar) consisting of about 58.5, 23.3, and 9.5 % of the total power produced, respectively. Fossil-fuels (primarily natural gas) in Ontario account for only 8.2 % of the electricity generation mix,[5] which is primarily used for peaking. As a result, less than 4 % of Ontario's greenhouse gas (GHG) emissions arise from electricity generation.[6] Because so few fossil fuels are used to produce electricity, and because there is potentially an oversupply of baseload electricity at present,[2] the carbon dioxide reductions that can be achieved by further decarbonization efforts in the electricity sector is relatively small. For these reasons among others, the province has decided not to construct new nuclear units for electricity purposes.[2] However, there is much room for improvement in Ontario's transportation-related emissions, which are about 58.7 Mt_{CO2e}/yr and account for almost 35 % of its total emissions.[6]

Canada has a particularly large supply of biomass in commercial production (roughly 143 Mt/yr, including agriculture).[7] In 2014, 1.8 Mt/yr of this biomass was in the form of wood pellets (a particularly useful form of non-food-competitive energy biomass), 90 % of which was exported (primarily to Europe) to be used as a biofuel there, with wood pellet exports growing quickly.[8] Ontario has the majority share of wood pellet production capacity, at about 1 Mt/yr, with the potential for additional growth in capacity in eastern Ontario[9] and southeastern Ontario to a lesser extent,[8] particularly in regions hardest-hit by pulp-and-paper industry declines. From a big picture perspective, it makes sense to consume more Ontario-grown biomass locally for bioenergy purposes rather than consuming it in Europe, since the negative environmental impact of trans-Atlantic shipping is by no means negligible. Therefore, by both diverting existing wood pellet production toward biofuel production in Ontario and increasing pellet production capacity for the same, it should be possible to reduce GHG emissions for both Ontario and the world, even accounting for the reduced biomass availability in Europe.

However, Ontario has another underutilized low-carbon energy resource: nuclear energy. Ontario has a long history of safely operating nuclear energy, the necessary technology expertise, the necessary regulatory infrastructure, a supply chain of domestic uranium which currently produces 22 % of the world's supply,[10] and a voting public that continues to accept nuclear power as the primary electricity driver in their province (though perhaps not in their own back yards). However, although the next generation (Gen IV) of Canadian nuclear technology is in development (the super critical water reactor CanDU design, or SCWR CanDU),[11] it has little prospect for use for electricity generation within Ontario in the near future. However, it has significant potential for use in fuel production, such as for the production of hydrogen[12] or for syngas,[13] which can be used to make synthetic gasoline, diesel,[14] and dimethyl ether (DME, a diesel substitute).[15] Since nuclear plants that produce fuels and not electricity do not have major issues associated with electricity transmission losses, they do not need to be located close to metropolitan areas, which can help alleviate public anxiety about nuclear plant proximity.

Therefore, we present the first biomass-gas-and-nuclear-to-liquids (BGTNL) polygeneration plant design available in the open literature to the best of our knowledge. We considered natural gas as a potential energy source both because it is readily

* *Author to whom correspondence may be addressed.*
E-mail address: tadams@mcmaster.ca
Can. J. Chem. Eng. 96:1853–1871, 2018

DOI 10.1002/cjce.23231
Additional supporting information may be found online in the Supporting Information section at the end of the article.
Published online 26 April 2018 in Wiley Online Library (wileyonlinelibrary.com).

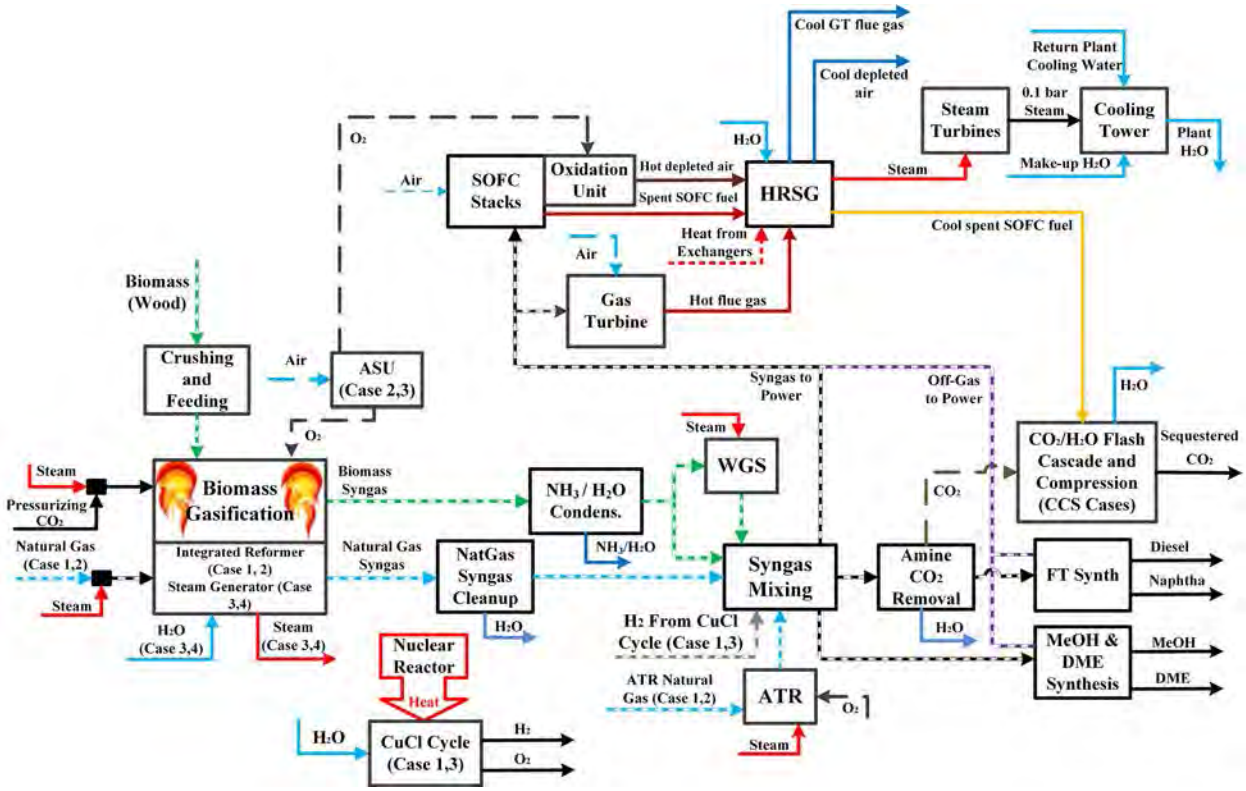

Figure 1. The BGNTL process superstructure used in this work.

accessible in Ontario, and because previous studies have shown that it is often preferable to use a combination of a fuel that produces hydrogen-rich syngas (e.g., natural gas) and a solid fuel that produces hydrogen-lean syngas (e.g., coal or biomass), rather than the coal/biomass alone,[16] particularly in the context of polygeneration.[17] We used chemical process modelling techniques to compute the necessary mass and energy balance flows and present them in this paper for a base case suitable for use in Ontario. We also provide, for the first time, an Aspen Plus v10 flowsheet containing the converged models as supplementary material.[1]

PROCESS AND SIMULATION METHODOLOGY

Process Overview

An outline of the proposed BGNTL process superstructure is shown in Figure 1, and specific details of each step can be found in later subsections. The process begins with biomass crushing and feeding to the gasifier. The woody biomass, CO_2, steam, and high purity O_2 (created in an air separation unit, or ASU) are fed to a downward entrained-flow gasifier to facilitate syngas production. Partial oxidation then occurs in the gasifier, and the raw syngas produced is cooled by one of two means: (1) by raising steam in a radiant steam cooler, or (2) by an integrated reformer (IR), which is composed of an integrated steam methane reformer (SMR) and radiant syngas cooler (RSC) with a similar design to that proposed by Ghouse et al.[18] In that case, the IR utilizes the heat from the raw syngas to reform a stream of natural gas into hydrogen-rich syngas, while the hydrogen-lean biomass-derived syngas leaving the gasifier is cooled. The two syngas streams are unmixed and processed separately downstream. The biomass-derived syngas is quenched using process water to around 200 °C.

The biomass-derived syngas does not need desulphurization because the sulphur content in the wood is so low, resulting in a sulphur content in the syngas of only about 50 ppm. Therefore, water (along with ammonia) can be directly condensed out of the biomass syngas. After this section, the syngas is mixed with gas-derived syngas from the RSC, as well as potentially other streams such as syngas coming from an autothermal reformer (ATR), nuclear-derived H_2 from a CuCl cycle, or shifted syngas from a water gas shift (WGS) reactor, depending on the case considered and the optimization results.

After syngas mixing, it is destined for one of three places. It is either mixed to a 2.01 H_2/CO molar ratio and sent to either the MeOH/DME section or the FT section; or, it is mixed in a non-specific H_2/CO ratio and sent to the power generation system (an amine-based CO_2 removal system is used prior to liquid fuel synthesis). The power generation system consists of either a gas turbine (GT) or a solid oxide fuel cell (SOFC) system for power generation. The power generation system includes a heat recovery and steam generation (HRSG) section for process steam needs and a bottoming cycle for additional electricity production from waste heat. An optional CO_2 purification and compression system is used to prepare captured CO_2 for pipeline transport for either sale or sequestration.

[1]Because of journal file size limitations, the simulation files have been deposited into the simulation repository at PSEcommunity.org. The direct link to the files is http://psecommunity.org/simfiles/ScottAdams2018.zip. The reader is encouraged to search the repository at PSCcommunity.org if the link is not working.

Table 1. Process cases considered in this work

Case	*Case Name*	*Woody Biomass Used*	*Natural Gas Used*	*Nuclear Energy Used*	*Biomass-syngas cooling method*	*CCS Used*
1.1	BGNTL-CCS-IR	YES	YES	YES	Internal Reforming	YES
1.2	BGNTL-CCS-SteamRSC	YES	YES	YES	Steam Generation	YES

In this work, we considered two different design structures, as shown in Table 1. Although the results for both cases will be shown in summarized form, detailed stream and unit operation results for only Case 1.1 will be shown in this work, since it demonstrates all aspects of the model conveniently. A future work will examine these cases in an optimization context.

Simulation Strategy and Basis of Comparison

Both cases shown in Table 1 were modelled utilizing a variety of process simulation tools in combination, including Aspen Plus v10, Matlab, ProMax, and gProms, as described in detail in later subsections. ProMax simulations were used for the sulphur and CO_2 absorption sections, which used their proprietary TSWEET physical property package. gProms simulations were used for the integrated reformer, and used various physical property models and correlations that were validated in prior work against experimental data, as described in prior work.[18] All other process section simulations were performed in Aspen Plus using the Peng-Robinson equation of state with the Boston-Mathias modification (PR-BM) property package, except for three cases: 1) pure water streams used the NBC/NRC steam tables; 2) flash calculations concerning CO_2-water phase equilibria at high pressures used the predictive Soave-Reidlich-Kwong package (PSRK), since prior work showed it to be more accurate than PR-BM under those conditions;[19] and 3) the DME/methanol separation sections used NRTL-RK. Matlab was used as a linking tool to facilitate automation and information transfer between the different software packages.

For a consistent basis-of-comparison in this example, the wood feed rate was fixed at 100 t/h (as received), the nuclear heat input was fixed at 117 MW, and the natural gas rate to the autothermal reformer was fixed at 664 MW_{HHV} for both cases, noting that the ratios of these energy feeds are subject to optimization. However, Case 1.1 contains an additional 169 MW_{HHV} of natural gas feed to the integrated reformer unit in the RSC (determined by the amount of heat available in the RSC), whereas Case 1.2 instead uses boiler feed water to make steam for electricity in the RSC. Each plant was designed such that all utility needs were produced on site, with no utilities imported, with the exception of water. The properties of the primary raw materials used in this work are shown in Table 2.

The mechanical equipment models used in this work (gas turbines, steam turbines, etc.) used the assumed parameters, as shown in Table 3.

Biomass Processing and Gasification Section

The as-received wood chips are first crushed to a maximum particle diameter of 1 mm, to achieve optimal mixing while gasifying.[22] Therefore, a crushing power of 0.02 kWe per $kWth_{HHV}$ of wood was assumed to crush the biomass to the required size.[22] The crushing itself was not modelled.

The modelled gasifier was a biomass steam pressurizing CO_2 and oxygen fed entrained flow gasifier. The system was modelled as a 0-D system in Aspen Plus, which considered the three stages of the gasifier: biomass decomposition, gasification, and cooling. The model strategy of Field and Brasington[23] and of Adams and Barton[19] (both developed for coal gasification) was adapted for pulverized wood chips by changing the feed properties accordingly. For brevity, the reader is referred to the latter work for a detailed description of the model. In short, the overall approach was to first model the decomposition of biomass into a multi-phase mixture of solid C, solid S, water, and H_2 and Cl_2 gases. Then, the gasifier output is estimated by assuming chemical equilibrium at 4.5 MPa and 1300 °C of the reaction of decomposed biomass with O_2, high pressure steam (HPS) fed at a rate of 2.8 % of the biomass mass flow rate,[24] and pressurizing CO_2 at a rate of 12 % of the biomass mass flow rate.[24] The effects of the low levels of ash that exist in biomass and the need for ash recycle is not taken into account in this work.[24] The O_2 flow rate was set such that the temperature of the gasifier was 1300 °C. It is also assumed that there is 100 % carbon conversion of the gasified biomass and that 2.7 % of the heat generated by the gasifier is lost to the surroundings.[24]

Table 2. Feedstock properties used in this work

Biomass Properties					
Ontario Cedar Wood Chips, As Received		*Proximate Analysis (wt%)*[20]		*Ultimate (wt% dry)*[20]	
HHV[20] (kJ/kg)	19804.82	Fixed Carbon	58.16	Carbon	48.62
LHV[20] (kJ/kg)	18790	Volatile Matter	39.94	Hydrogen	5.991
Average MW of ash[21]	65.15	Ash	1.90	Nitrogen	0.478
Mole fraction F_e2O_3 in ash[21]	0.02613	Moisture	8.00	Sulphur	0.005
				Oxygen	43.006
				Chlorine	0.209
Natural Gas Properties					
Conditions at plant gate		*Mole Fractions at Plant Gate*[14]			
Temperature (°C)	30	Methane	0.939	*n*-Butane	0.004
Pressure (MPa)	3.0	Ethane	0.032	CO_2	0.010
		Propane	0.007	N_2	0.008

Table 3. Assumed efficiencies for mechanical unit operations in the Aspen Plus models used in this work

Unit Operation	Isentropic Efficiency	Polytropic Efficiency	Mechanical Efficiency	Reference
Compressors		0.85	0.94	Clausen et al.[24]
Gas Turbines	0.898		0.988	Khojestah Salkuyeh and Adams[15]
Expanders	0.898		0.988	Khojestah Salkuyeh and Adams[15]
Steam Turbines	0.875		0.983	Khojestah Salkuyeh and Adams[15]
Pumps			0.80	Khojestah Salkuyeh and Adams[15]

Two different RSC approaches were considered (see Table 1), one with an IR and one with only a steam generator, shown in Figure 2 below. The classic steam generation version uses a simple heat exchanger model in Aspen Plus that computes the cooling duty necessary to achieve a syngas output temperature of 780 °C, and computes the rate of boiler feed water at 101 °C and 5.2 MPa necessary to achieve it such that HPS is created at 500 °C.

The model of the IR was based on the design and multi-scale model developed by Ghouse et al.[18] for a SMR within the RSC of a coal-fed entrained flow gasifier. For brevity, the reader is referred to Ghouse and Adams[25] and Ghouse et al.[18] for full details, and the design and the model is instead summarized here. The reformer consists of two concentric circular rings of vertical tubes inside the shell of the radiant syngas cooler, offset from each other to maximize lines-of-sight to best facilitate radiant heat transfer. The gasifier syngas exhaust flows downward on the shell side of the RSC, and the shell is lined with refractory to prevent heat loss. Each tube is packed with SMR catalyst, with the steam and pre-reformed natural gas feed at the top of the tubes, thus operating in co-current flow (which helps with heat management issues). The gasifier section contains a neck that allows solids and slag to fall through the middle of the tube rings to minimize contact with the tubes.

The pre-reformer shown in Figure 2 (left) was modelled in Aspen Plus using an REQUIL block at 3.44 MPa and adiabatic conditions using the same approach described in Adams and Barton.[26] The steam flow is sufficiently large and hot enough to reform the higher hydrocarbons adiabatically, but not the methane.[26] Therefore, the pre-reformer model assumes 100 % conversion of the ethane, propane, and butane steam reforming reactions, and assumes chemical equilibrium of the water gas shift and steam methane reforming reactions, which have relatively little conversion. The relatively high steam to carbon ratio in the reaction mixture ensures no carbon deposition.[26]

The model of the IR portion is non-linear, two-dimensional, heterogeneous, and considers axial variations in temperature

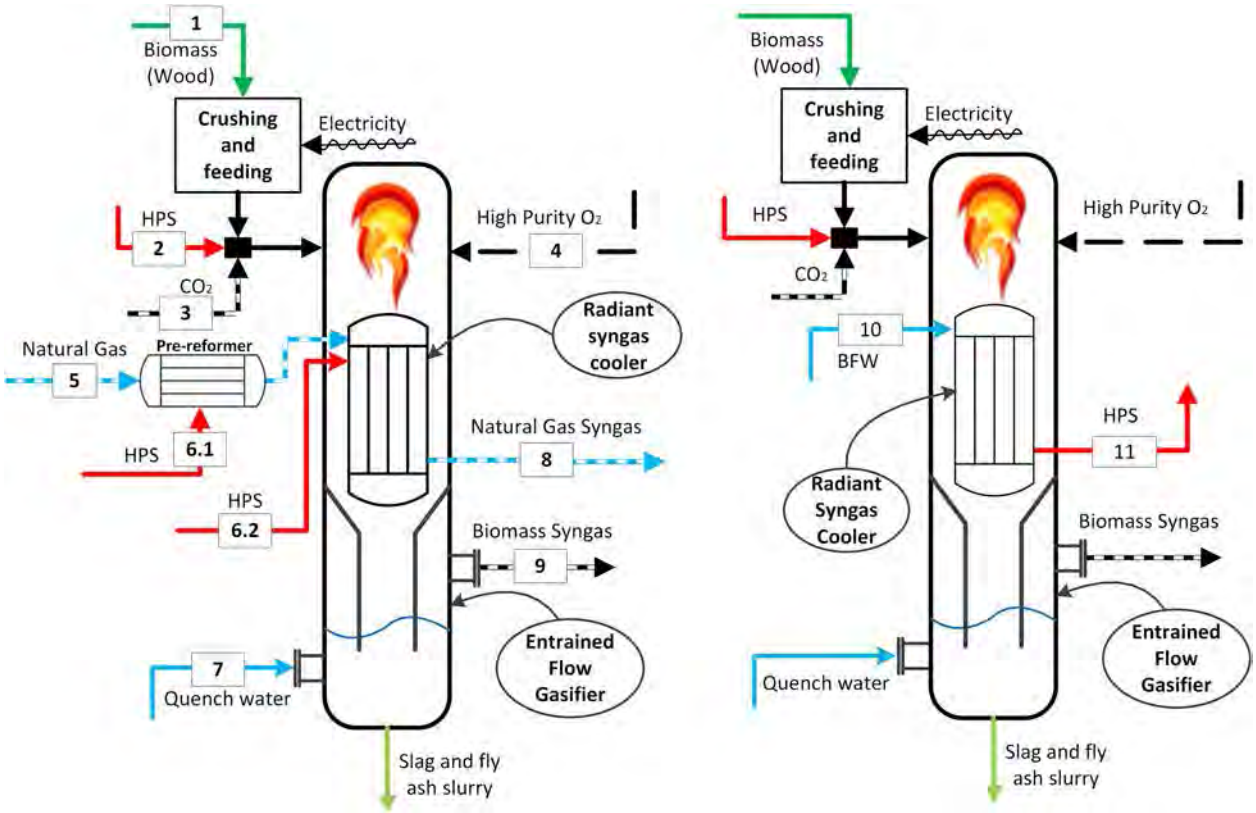

Figure 2. The two radiant syngas cooling options considered in this work: (left) integrated radiant syngas cooling with steam methane reforming, and (right) classic steam generation only.

and composition in the shell and tube gas phases on the dm scale, axial and radial temperature differences in the tube walls on the cm scale, and temperature and composition variations in the catalyst particles on the mm scale. The model considers radiative and convective heat transfer between the shell and tube walls, homogeneous reaction on the shell side (such as water gas shift at high temperatures), conduction within the tube walls, convection within the tube side gases, reaction and diffusion within the catalyst particles, conduction through the refractory walls, and heat losses to the atmosphere. The model used in this work was modified from the original model of Ghouse et al.[18] by changing the syngas feed composition to match the biomass-derived syngas, as predicted from the Aspen Plus gasifier model described above, but otherwise was unchanged. The design parameters chosen for the IR portion were 137 reforming tubes each 20 m in length and 8 cm in diameter inside of a 4.5 m diameter shell. These were manually selected to work well with a gasifier consuming 100 t/h of biomass feed, balancing the trade-offs between cooling duty, methane conversion, and pressure drop. The model was implemented as a set of roughly 100 000 partial differential algebraic equations into gProms and was solved using a finite difference method. Although the model is dynamic, only steady state solutions were used in this work.

Although the design of the IR was fixed, the flow rates of the natural gas and reforming steam were allowed to vary from case to case based on system-wide optimization. Because the gProms model had convergence times that were too long (about 1 h per run) to be included in an optimization loop, we created a reduced order steady-state model (ROSSM) from the rigorous gProms model that could be rapidly used within Aspen Plus during optimization without the need to call gProms. To describe briefly, we performed 80 simulation runs using Latin hypercube sampling within a bounded state space of two independent variables, with 60 runs as training data and the rest as testing data. We examined several candidate polynomial (linear-in-the-parameters) models for each of the dependent variables of interest and found that 1st order (linear) models did not represent the nonlinearities well, that 2nd order models had excellent R^2 values for both training and testing sets, and that 3rd order models introduced some spurious curvature and so were rejected. The final models ROSSMs selected for the work have the following structure:

$$Z_i = a_{1,i} + a_{2,i}\frac{F_{NG}}{\overline{F_{NG}}} + a_{3,i}\frac{R_{S:C}}{\overline{R_{S:C}}} + a_{4,i}\left(\frac{F_{NG}}{\overline{F_{NG}}}\right)^2 + a_{5,i}\left(\frac{R_{S:C}}{\overline{R_{S:C}}}\right)^2 + a_{6,i}\left(\frac{F_{NG}}{\overline{F_{NG}}}\right)\left(\frac{R_{S:C}}{\overline{R_{S:C}}}\right) \quad (1)$$

where Z_i are the model outputs for variable i, as shown in Table A1 in the appendix, and $a_{j,i}$ are the model coefficients for coefficient j for output variable i, as shown in Table A1. F_{NG} is the flow rate of natural gas in kmol/h, $R_{S:C}$ is the steam-to-carbon ratio (the molar flow rate of steam divided by the molar flow rate of methane), and $\overline{F_{NG}}$ and $\overline{R_{S:C}}$ are normalization factors (the average of the range of independent variables used in identifying the model). The model was implemented in Aspen Plus using a Calculator block in combination with an RSTOIC model of the reforming equations. The ROSSM model equations were solved analytically by fixing two degrees of freedom: the methane conversion at 80 % (a conservative value for SMR),[18] and the cooling duty at the value required to cool biomass-derived syngas from the gasifier to 780 °C. Although it would be preferable to allow these variables to be subject to optimization, we found it necessary to fix them to arrive at manageable optimization times.

An overview of the IR section model, as implemented in Aspen Plus, is shown in Figure 3.

Air Separation Unit

The air separation unit (ASU) is not directly modelled in this study. However, the power consumption associated with producing O_2 along with a corresponding stream of waste N_2 was considered using the results reported by Clausen et al.,[24] such as 1 MWe consumed in the ASU per 1 kg/s of O_2 produced at 0.1 MPa. When further compressing the O_2 to 1.29 MPa with two stage compression and intercooling (as modelled in Aspen Plus), the total power required becomes 1.333 MWe per 1 kg/s of O_2 produced at 1.29 MPa.

Ammonia Removal

After the gasifier, the biomass-derived syngas is cooled to about 40 °C such that most of the water is condensed out, carrying trace ammonia contained in the syngas with it. The remaining syngas is sent to the syngas mixing section. This is modelled with a FLASH2 block in Aspen Plus using the PR-BM equation of state, and shown in Figure 4. Although the cleaning of the recovered sour water is not included in the model, it will be included in the economic analysis in Part II of this work.

Syngas Mixing and Upgrading

The syngas mixing section is the area that mixes and adjusts the syngas to a desired H_2/CO ratio or sends it to power generation. Additional unit operations that are present in this section are the WGS reactor and the ATR reactor, which are discussed next.

The purpose of the water gas shift reactor (WGSR) section is to upgrade syngas coming from the biomass gasifier, which has a low H_2/CO ratio to a higher ratio of 2.01, since this syngas is destined for methanol and Fischer-Tropsch chemical production.[16] The WGSR was modelled as a set of three adiabatic REQUIL reactors in series, which assumes chemical equilibrium using a 20 °C approach temperature. The sequencing of reactors exploits the fast kinetics of the first two reactors, but utilizes the favourable low temperature equilibrium of the reaction system at the end.[28] The low temperature reactor exploits the equilibrium moving more towards the products, namely hydrogen gas. Steam is added to the entrance of the first reactor such that a syngas H_2/CO ratio of 2.01 is obtained at the exit of the last reactor. A schematic of the WGSR section is shown below in Figure 5. Note that the flow rate of this section varies widely between simulation cases. In practice, the high temperature reaction takes place between 300–450 °C over a $Fe_2O_3/Cr_2O_3/CuO$ catalyst. The low temperature reaction occurs over a $Cu/ZnO/Al_2O_3$ catalyst between 120–300 °C. The intercooler temperature output settings chosen were about 327 and 232 °C for the first and second intercoolers, respectively. These are subject to optimization but the impacts of changes in temperature on the design and its performance are minimal.

For some cases, an ATR section is used to create hydrogen-rich syngas derived from natural gas, steam, and oxygen (this is a separate reactor from the SMR integrated with the gasifier's

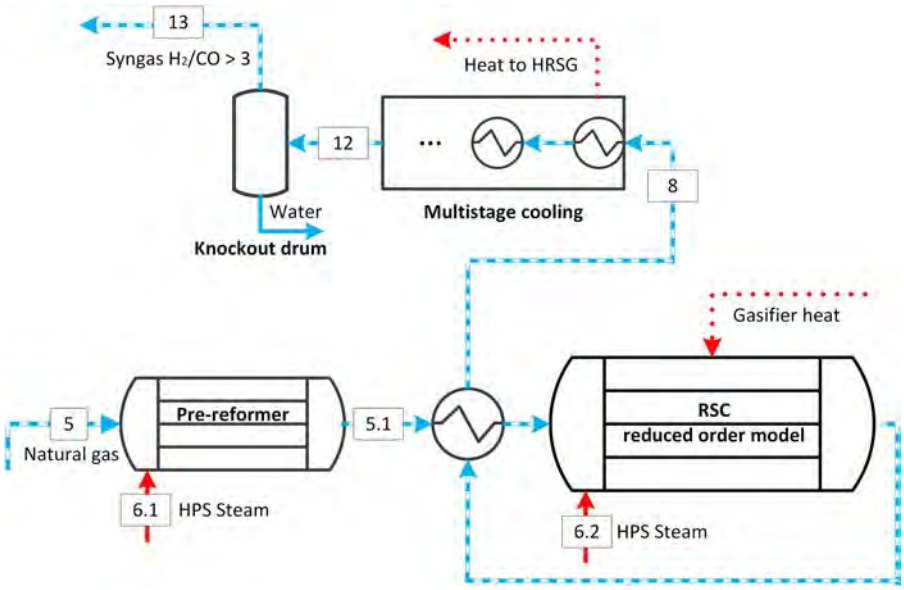

Figure 3. The IR section, as modelled in Aspen Plus.

radiant cooler). The hydrogen-rich syngas can be mixed with biomass-derived syngas for power or to increase the hydrogen content for fuels and chemical production. An outline of the model is shown in Figure 6. The system consists of a pre-reformer, the ATR, a system of heat exchangers, and a flash drum for water removal. The pre-reformer and the main reformer were modelled as adiabatic equilibrium reactors in Aspen Plus. The reactors operated at 3.0 MPa due to the availability of natural gas at this pressure and the need for high pressure syngas downstream. The assumed pressure drop of the pre-reformer and main reformer were 40 and 60 kPa, respectively.[26] The purpose of the first reformer is to pre-reform the syngas and totally reform the largest hydrocarbons (C_2–C_4), while the purpose of the second reformer is to oxidize a portion of the methane in the natural gas to provide the heat to drive the endothermic methane steam reforming reaction. The amount of high pressure steam that was added to each reformer was selected according to the methodology of Adams and Barton[16] to prevent carbon deposition, provide adequate methane conversion, and avoid excessive steam use. The amount of oxygen added to the system was chosen so that the outlet temperature of the main reformer was 950 °C. The pre-reformer inlet was preheated to 500 °C and the main reformer inlet was preheated to 840 °C.

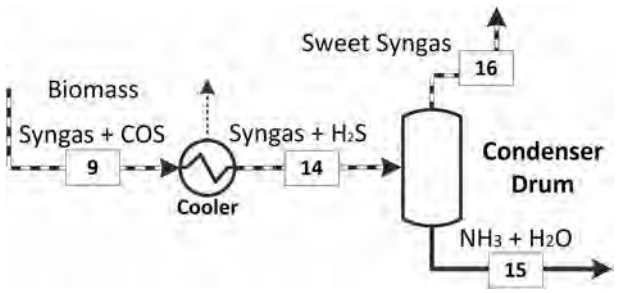

Figure 4. The ammonia removal section, as modelled in Aspen Plus.

For some cases, hydrogen was produced using the copper-chlorine (Cu-Cl) cycle from nuclear energy and used for syngas upgrading or for hydrocracking in the FT section. The nuclear reactor and Cu-Cl cycle were not modelled in this study, but have been extensively modelled in previous works using Aspen Plus,[29–31] with those results incorporated herein. The Cu-Cl cycle was developed at the Ontario Institute of Technology in collaboration with Atomic Energy of Canada Limited,[30,31] and is particularly suitable for integration with the GenIV CanDU SCWR design.[32] The Cu-Cl cycle has several variations, one of which is the 5-step cycle, considered in this work, is shown in Figure 7, and consists of the following steps:

Step 1: Hydrogen generation: $2Cu(s) + 2HCl(g) \rightarrow 2CuCl(l) + H_2(g)$ at 430–475 °C.

Step 2: Electrochemical CuCl splitting: $2CuCl(s) \rightarrow Cu(s) + CuCl_2(aq)$ at ambient temperature.

Step 3: Flash drying: $CuCl_2(aq) \rightarrow CuCl(s)$ at 150 °C.

Step 4: HCl production: $2CuCl_2(s) + H_2O(g) \rightarrow CuO \cdot CuCl_2(s) + 2HCl(g)$ at 400 °C.

Step 5: Oxygen production: $CuO \cdot CuCl_2(s) \rightarrow 2CuCl(l) + \frac{1}{2}O_2(g)$ at 500 °C.

In this work, it is assumed that some of the heat from the CanDU SCWR is used for the heating step for Step 4 (via an intermediate loop with helium as the heat carrier), with the remainder of the SCWR heat used for power generation explicitly for electrochemical splitting (Step 2) and the balance of the nuclear plant needs, as shown in Figure 8. For this work, we assume that no additional electric power comes from nuclear energy and the Cu-Cl cycle is sized only to produce the necessary hydrogen.

It was assumed that the CuCl cycle acts as a stand-alone external utility, and the water required is solved by mass balance. It was assumed that it took 145 MJ of thermal energy and 60.7 MJ of electric energy to generate 1 kg of hydrogen.[29] However, assuming the thermal efficiency of the SCWR is 50 %, a total of 266 MJ of thermal energy from the SCWR is required to generate 1 kg of H_2 in this process,[30] resulting in an efficiency of energy conversion of around 44 % by HHV.

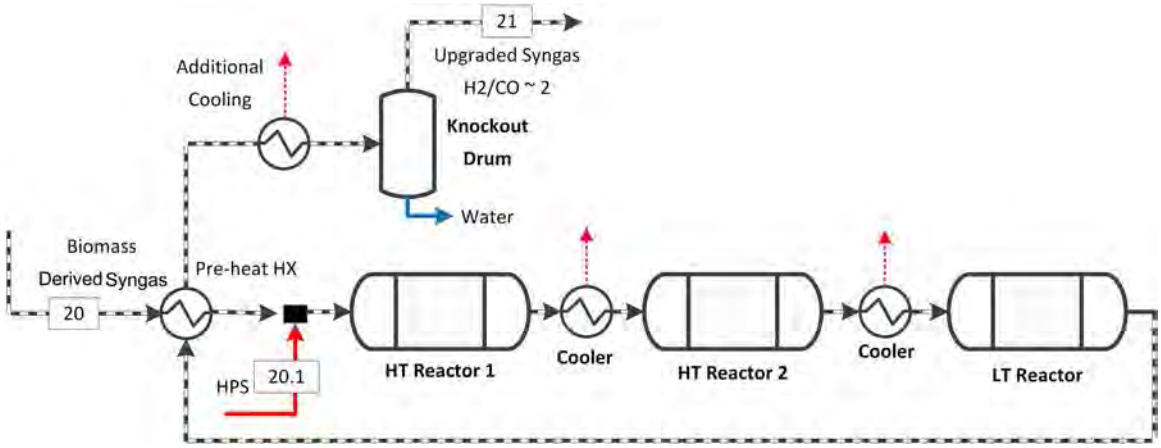

Figure 5. The Aspen Plus model of the WGS section.

This compares well to other advanced carbonless strategies for making hydrogen, such as advanced water electrolysis via high temperature heat (49 %), but it is less efficient than classic steam methane reforming (86 %).[41] The oxygen generated by the CuCl cycle is used to displace the oxygen generated by the ASU, making its size and energy consumption smaller. The outlet conditions of the O_2 and H_2 from the CuCl cycle are assumed to be 20 °C and 1.0 MPa.[32] For details about the Cu-Cl process and how it can be integrated with a CanDU SCWR, the reader is referred to Rosen[32] and Tsvetkov,[33] respectively.

Figure 9 shows the syngas upgrading section superstructure. The various stream split percentages, such as the amount of syngas used for liquid fuels production (and which kind of fuel) versus power generation, the amount of diversion for the water gas shift section, and the amount of natural-gas derived syngas used for blending or for power, are all design degrees of freedom. If both nuclear heat and FT are used, all of the hydrocracker H_2 needs in the FT section are met through stream 26.1.

Power Generation Section

The power generation section contains two options, one using SOFCs and the other with gas turbines, each with a bottoming steam cycle. Both systems are fueled by a blend of syngas from upstream units and off-gases from downstream units, and a splitter allows a portion of the syngas to be sent to either section as a design degree of freedom, as shown in Figure 10.

The SOFCs are powered by syngas in the anode with ordinary air in the cathode, each at about 2.0 MPa pressure. The CO and H_2 present in the feed is electrochemically oxidized directly into CO_2 and H_2O by the reaction of oxygen ions, which migrate from the cathode to the anode through the solid electrolyte barrier. This prevents N_2 from entering the fuel exhaust, thus allowing two separate outlet streams. The hot cathode exhaust is used for additional electricity in a Brayton cycle, and the anode exhaust, which still contains some CO and H_2, is further oxidized catalytically using O_2 from the ASU. This results in a stream of only CO_2 and H_2O, which can be separated through a series of flash drums, thus facilitating low-energy CO_2 capture. The CO_2 is captured at high pressure (1.9–2.0 MPa) and the water is recovered at high purity at atmospheric pressure. The captured CO_2 is further compressed in a compression and sequestration section described later.

The Aspen Plus model for the SOFC system was originally developed in previous works and fully described there.[19,26] The key assumed parameters are that the system achieves a voltage

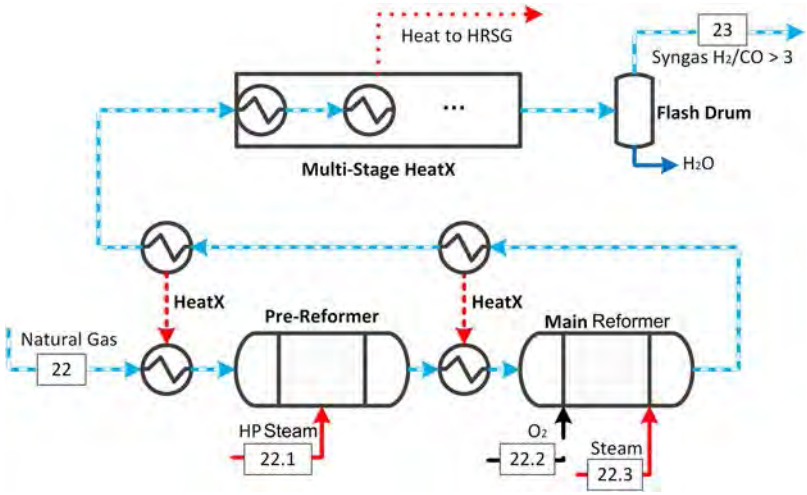

Figure 6. The Aspen Plus model of the ATR section.

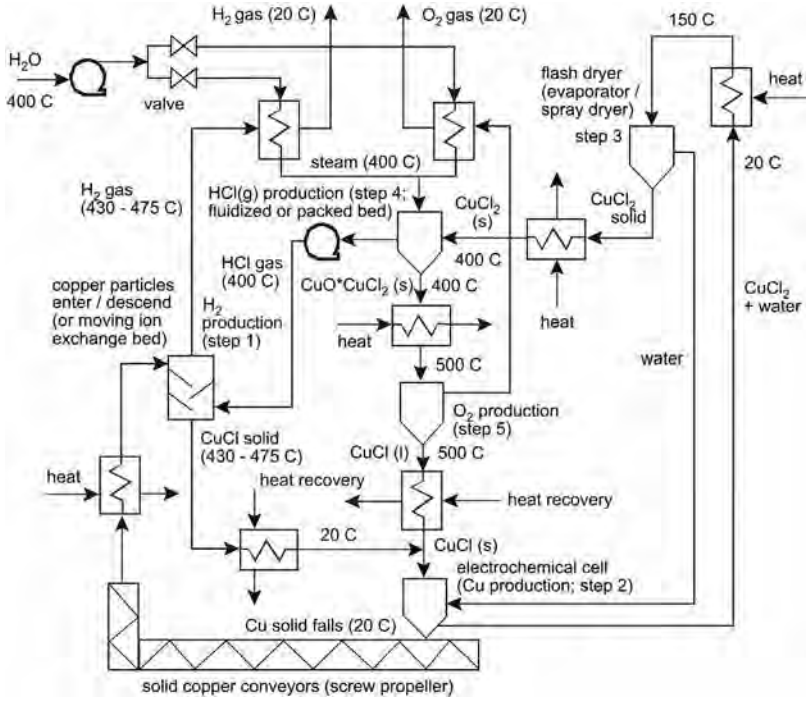

Figure 7. The Cu-Cl cycle, reprinted from Rosen[32] with permission from Elsevier.

of 0.86 V, has a DC to AC inversion efficiency of 96 %, and that 5 % of all energy released by oxidation in the SOFC is lost as waste heat. An integrated cooling system keeps temperatures in the 910–1030 °C range, which is recovered in the HRSG. The post-anode catalytic oxidation system used stoichiometric air from the ASU with a boost compressor and was modelled assuming 99 % conversion of energy chemicals (H_2, CO, CH_4, methanol, ethanol, DME, and methyl formate) in an adiabatic RSTOIC block. The Aspen Plus model for the flash drum purification section is not shown in Figure 10 for brevity, but is described fully in Adams and Barton[19] and accounted for in the analysis.

The gas turbine in this work (also shown in Figure 10) was modelled using RGibbs and compressors/turbine blocks in Aspen Plus. The inlet pressure to the gas turbine was 2.1 MPa, and 9 % excess O_2 (in the form of air) was added to the gas turbine for combustion. A portion of this air stream was split and sent to mix with the combusted fuel to maintain a safe operating outlet combustion temperature.[16,24] In addition, waste N_2 was mixed from the ASU to dilute the incoming fuel stream and to achieve a lower heating value of 4.81 MJ/Nm^3.[16] The electrical conversion was also assumed to be 100 % efficient for the gas turbine,[24] while the mechanical conversion used the values noted in Table 3. The spent fuel is then sent to the HRSG section for heat recovery.

Carbon Dioxide Removal from Syngas

This section uses MDEA to remove CO_2 from syngas prior to use in the FT section. This step is needed because the FT catalyst can tolerate no more than 5 % inert gas content in the feed,[34] and other inert chemicals (such as N_2) are much harder to remove. In addition, much of the remaining H_2S left in the syngas is also be absorbed along with the CO_2. The feed to the CO_2 removal section is a mixture of blended syngas from upstream with recycle FT off-gases from downstream (including a recycle compressor).

This process was modelled in ProMax according to the procedure described by Adams et al.,[27] utilizing the TSWEET

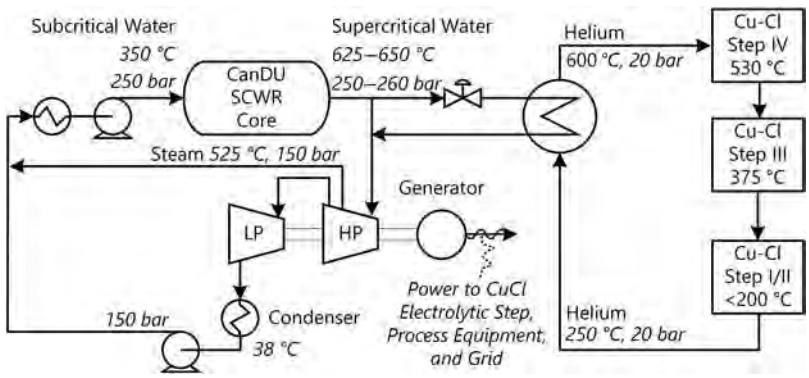

Figure 8. The CanDU SCRW reactor integrated with a Cu-Cl cycle, based on the original drawing in Tsvetkov.[33]

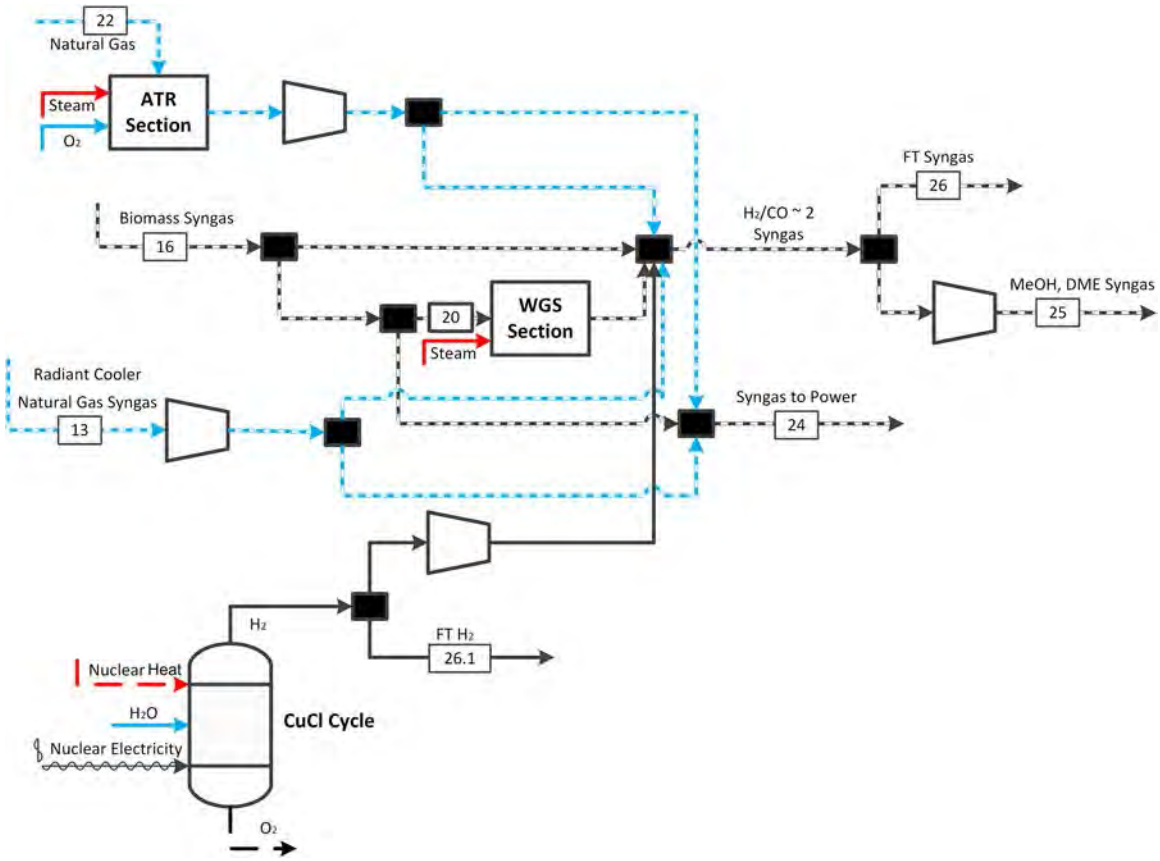

Figure 9. The Aspen Plus model of the syngas upgrading section. The Cu-Cl cycle is implemented as a RYield block to represent the net effects of the full cycle.

kinetics property package, as shown in Figure 11. The CO_2 removal process uses a classic configuration containing a contacting absorption column and regenerative stripper column. The absorption column operates at high pressure (15 ideal stages/45 actual trays: 3.8 MPa pressure at the top and 3.9 MPa bottom), while the stripper column operates at a relatively low pressure (10 ideal stages/30 actual trays: 180 kPa at the top and 200 kPa at the bottom). In addition, low pressure steam is used to heat the bottom of the column and cooling water is used in all of the cooling blocks.

A ROSSM was constructed from the ProMax model such that it could be incorporated into the Aspen Plus flowsheet using a

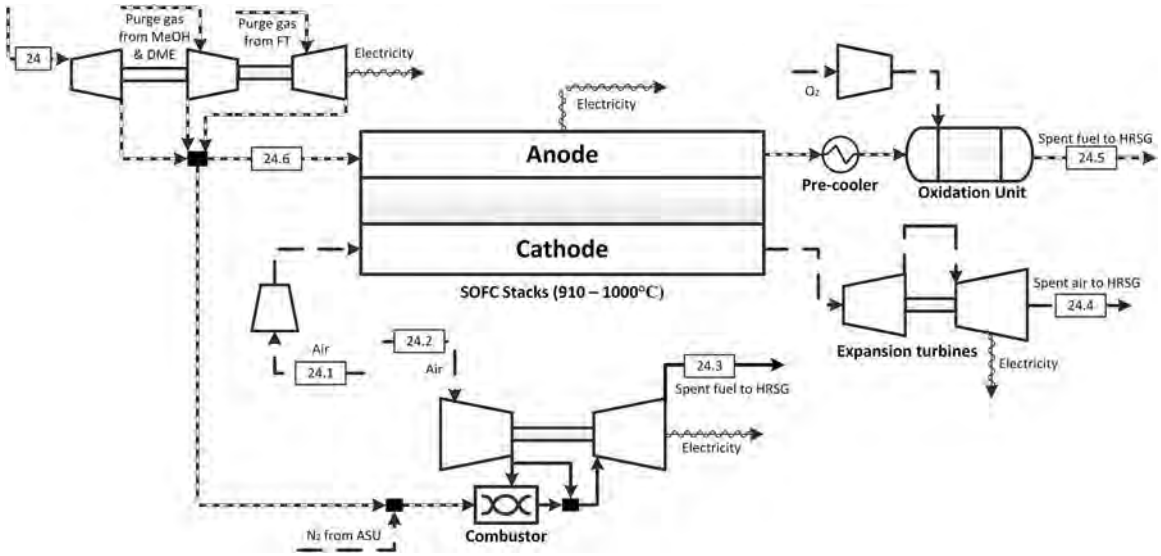

Figure 10. The power generation section superstructure. The O_2 feed for the SOFC post-oxidation unit is produced by the ASU.

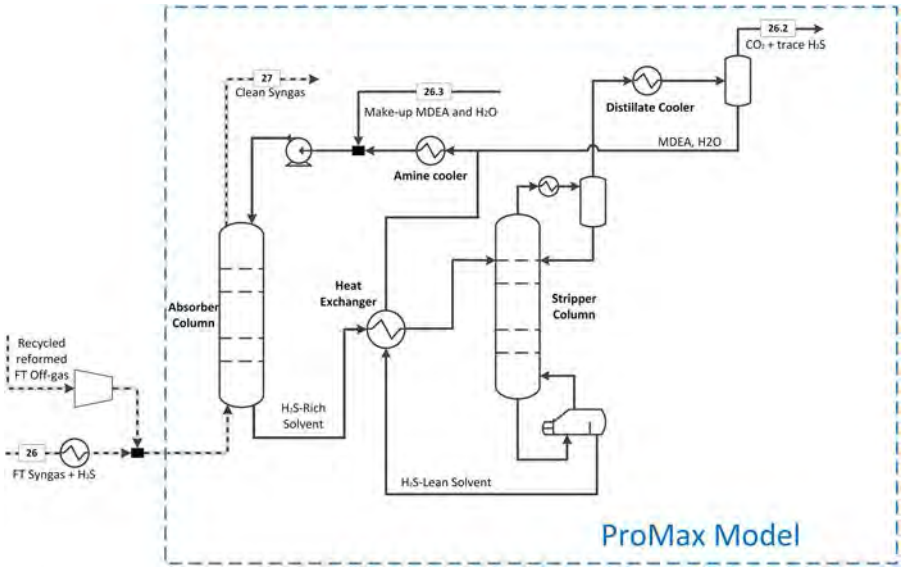

Figure 11. The section for removing CO_2 from syngas destined for liquid fuel production. The compressor and mixer are modelled in Aspen Plus, and the balance are modelled in ProMax.

combination of Calculator and SEP blocks, making execution fast within Aspen Plus. The ROSSM is suitable for use only in the range of CO_2 concentrations and syngas flow rates encountered in this study, and is not generalizable to other applications. It was found that a linear model was sufficient for predicting key performance parameters, such as makeup solvent flow rates and heat exchanger duties, with higher order polynomials achieving little improvement. The model was trained with 55 simulation points (spaced evenly with just one independent variable, the flow rate of CO_2 in the feed stream) with 20 additional simulations used as the testing set. Each ProMax simulation was defined such that solvent flow rates were adjusted so that 90 % of the CO_2 was removed from the syngas. The resulting model is described in detail in appendix Table A2. The linear ROSSM describes the ProMax model very accurately for key parameters such as heat exchanger duties. Although it is less accurate at predicting makeup solvent flow rates (maximum 5 % error), those flow rates have a very minor impact on the economics and so it is acceptable.

Fischer-Tropsch Section

The FT section is shown in Figure 12. Upstream syngas with an H_2/CO ratio of 2 is sent to the FT cobalt-based reactor where it is pre-heated to 240 °C and reacted at 3.6 MPa to generate hydrocarbons with hydrocarbon up to 60. The model of Adams and Barton[16] was used for this section, which is described fully in that work and so is described here only briefly. The model for the FT reactor considers only straight alkyls, not branched, and for hydrocarbons pentane and higher, an Anderson-Schultz-Flory distribution with $\alpha = 0.92$ and a CO conversion of 65 % is assumed. Lower hydrocarbons have assumed product mixture concentrations as follows: CH_4 at 5 mol%, C_2H_4 at 0.05 %, CO_2, C_2H_6, C_3H_8, C_4H_{10} at 1 %, and C_3H_6 and C_4H_8 at 2 %. The model considers most of the hydrocarbons as separate chemicals, but larger hydrocarbons above a carbon number of 31 use representative chemicals to represent a group (for example, C_{31} through C_{32} are modelled as $C_{32}H_{66}$).

Once the FT products exit the reactor, they are subsequently cooled by two 3-phase flash tanks, which separate water destined for water treatment into two groups: the lights (naphtha (C_5–C_{11})) and heavies (C_{12}–C_{20}). These are sent to the refinery column, while off-gasses are sent to an ATR (which operates at 950 °C and at an exit H_2/CO ratio of 2) in the FT section for reforming. The off-gasses are then either recycled back to the CO_2 removal section or sent to power generation as a decision variable. The light and heavy components then enter the refinery column, which is modelled in Aspen Plus using the PetroFrac block. The column has 20 stages with a top pressure of 270 kPa and a bottom pressure of 340 kPa. The reboiler operates at 430 °C and the condenser operates at 38 °C. In addition, the following ASTM design specification for the tower was used: 95 % vol: gasoline 170 °C and diesel 340 °C.

After the refinery column, the heavier hydrocarbons are sent to the hydrocracker where the carbon chains are broken into smaller chains for fuel production. Hydrogen is added to the hydrocracker either by pressure-swing absorption, where a portion of the FT feed has its hydrogen stripped from it for use in the hydrocracker, as indicated in Figure 12, or by H_2 generated in the CuCl cycle if the nuclear option was chosen in the superstructure. The hydrocracker model uses a plug-flow kinetic model, with more details described in Adams and Barton.[16] The separator following the hydrocracker was not modelled since it has a small impact on plant costs, and instead it is assumed that hydrocarbons C_{11} and smaller leave through the distillate and heavier hydrocarbons leave through the bottoms. Similarly, the product decanters assume perfect water removal for simplicity.

Methanol and Dimethyl Ether Synthesis

The methanol and DME section is shown in Figure 13. This section produces methanol and DME from $H_2/CO = 2$ syngas with two separate reaction pathways. The model for this section was adapted from the model developed by Khojestah Sulkuyeh and Adams[15] and the details are fully described in that work and so it is summarized here only briefly. The first step in this process is methanol synthesis over a $Cu/ZnO/Al_2O_3$

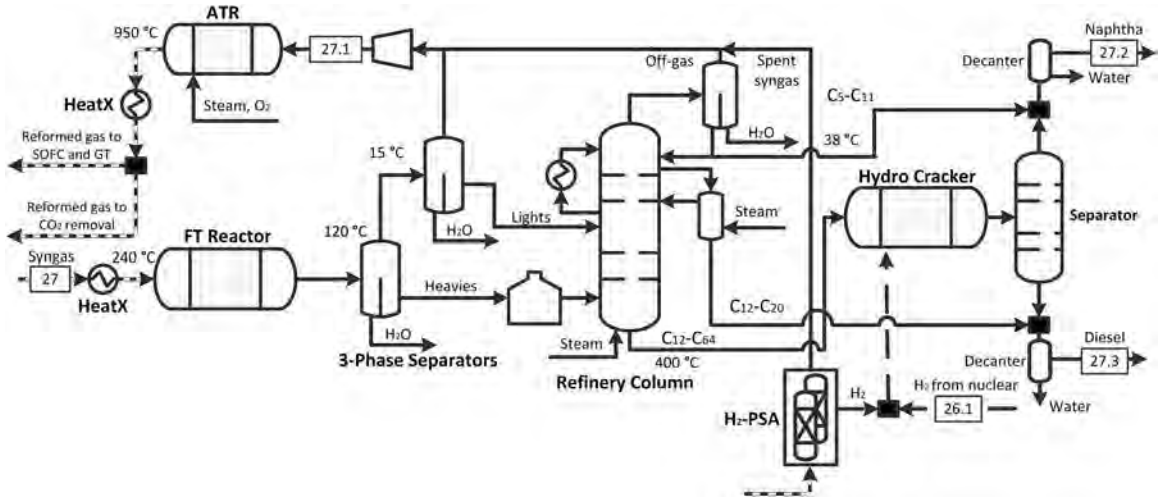

Figure 12. The model for the FT section of the superstructure.

catalyst (with simultaneous water gas shift reaction) in a reactor. The reactor model uses the Aspen Plus plug flow reactor model with Langmuir Hinshelwood Hougen Watson (LHHW) kinetics.[35] It considers the methanol synthesis reaction, the water gas shift reaction, and the formation of ethanol and methyl formate, and operates adiabatically with an exit temperature of 240 °C.

The unreacted syngas is then cooled down to 35 °C and is flashed in a flash drum (mostly unreacted gases such as N_2, CO, and H_2). A portion of the off-gas is recycled back to the start of the reactor and the rest sent to the power generating section. After the liquid methanol exits the first drum, it is distilled in a methanol recovery unit, which acts as a second light gas removing column. This column was modelled using a RadFrac block in Aspen Plus with 20 equilibrium stages using the NRTL-RK property method. The off gases of the methanol recovery column are then sent to the power generating section. The methanol purification column then purifies the incoming methanol to 99.5 % mol purity, with the bottom of the column being mostly water. This column was modelled as a RadFrac column using 40 equilibrium stages and the NRTL-RK property package. After the methanol purification column, a portion of the methanol is split for sale (a decision variable) and the remainder is sent to DME synthesis.

The portion of the methanol that is sent to DME synthesis is first pressurized to 5.6 MPa and sent to a single-pass DME reactor operating at 280 °C and 5.6 MPa.[24] The reaction takes place in the DME reactor over a $\gamma - Al2O3$ catalyst, considering the dehydration reaction kinetics of Bercic and Levec.[36] DME is then recovered in the DME purification column, which is modelled using RadFrac with 30 equilibrium stages, utilizing the NRTL-RK package. The DME is purified to 99.5 mol% at the top of the column and the bottom of the column is recycled back to the methanol purification column.

Heat Recovery and Steam Generation

The purpose of the HRSG section is to take waste heat from the plant and generate various pressures of steam for additional power production and steam supply demands across the plant. There are three levels of steam used in this work: high pressure (HP) (500 °C, 5.0 MPa), medium pressure (MP) (300 °C, 2.0 MPa), and low pressure (LP) (180 °C, 500 kPa) steam. Various parts of the process utilize these different levels of steam, and steam demand outlets are made for each steam pressure based on plant demands. Minimum approach temperatures of 10 °C are used when constructing the various heat exchangers across the plant.[37] The excess steam that is not consumed by the plant is sent through 3 steam turbines, which generate additional power for the plant. In addition, boiler feed water heating and deaerating are taken into consideration when modelling the HRSG plant. The heat recovery section is shown in Figure 14.

CO_2 Compression and Sequestration

This section focuses on compressing CO_2 from various parts of the plant and sequestering it at 15.3 MPa pressure. This stage is particularly energy intensive as there are multiple cooling steps involved and large power demands from the multiple compressors that are involved. This section is modelled using the PSRK equation of state as it more accurately models the equilibrium of water and CO_2 in the liquid and gas phases at the relevant pressures of interest.[19] The various captured CO_2 streams are mixed at different stages of the compression sequence depending on their available pressure levels. The multi-stage compression models in Aspen Plus used cooling water to cool the interstage compressor outlets to 30–80 °C to both help with water removal (using flash drums) and to ensure compressor temperatures did not rise above 200 °C. Once CO_2 has reached supercritical pressures, it is pumped to 15.3 MPa for pipeline transport. The upstream CO_2 capture sections are designed to ensure that the purity of CO_2 is sufficient for most existing CO_2 pipelines.[19] The process is shown in Figure 15.

Cooling Tower Section

The cooling water section was modelled in this work as a two-stage equilibrium RadFrac column in Aspen Plus.[38] External air was blown through the tower to remove the heat of the incoming return cooling water (~50 °C) from the plant. Some of the water escapes as water vapour through the top of the tower; as such, makeup cooling water is added to the plant return water, which is around 30 °C. The incoming air is assumed to be 20 °C. In addition to the cooling tower, there are other utilities that require extra

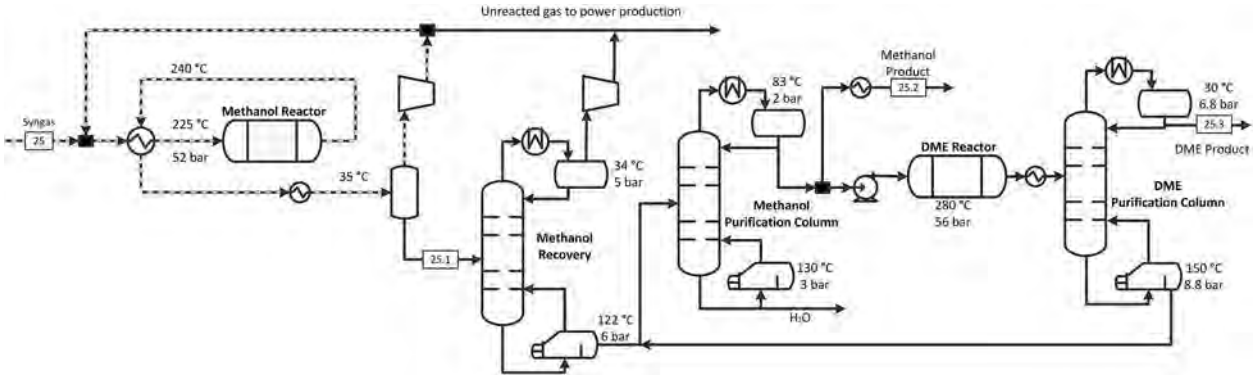

Figure 13. The model for the methanol and DME synthesis section of the superstructure.

cooling, so chilled water is used for these streams. The cooling water streams were modelled as utility streams with temperature inlet and outlet of 7–32 °C.[37] The model is summarized in Figure 16.

SIMULATION RESULTS

Base Case Results

As a demonstration of model capabilities, two base case simulations were run for the two corresponding design cases shown in Table 1. The decision variables for these cases, such as how much syngas to divert to liquid fuels or power generation, and how much methanol to keep as a product and how much to use for DME synthesis, were all fixed to approximately the middle of their feasible ranges. This creates a sort of "average" plant, which is suitable for a base case because it demonstrates all aspects of the superstructure at reasonably large sizes. It is certainly not optimal, but the optimal design will be very different depending on the objective function (i.e. environmental, economic, or both), market conditions, and business-related constraints. These optimality issues will be discussed in Part II of this work.

Sample stream conditions for Base Case 1.1 are shown in Table 4, which includes all of the advanced options (nuclear hydrogen production, integrated steam methane reforming and syngas cooling, and CO_2 capture and sequestration), and includes a mix of all possible products (SOFC-generated

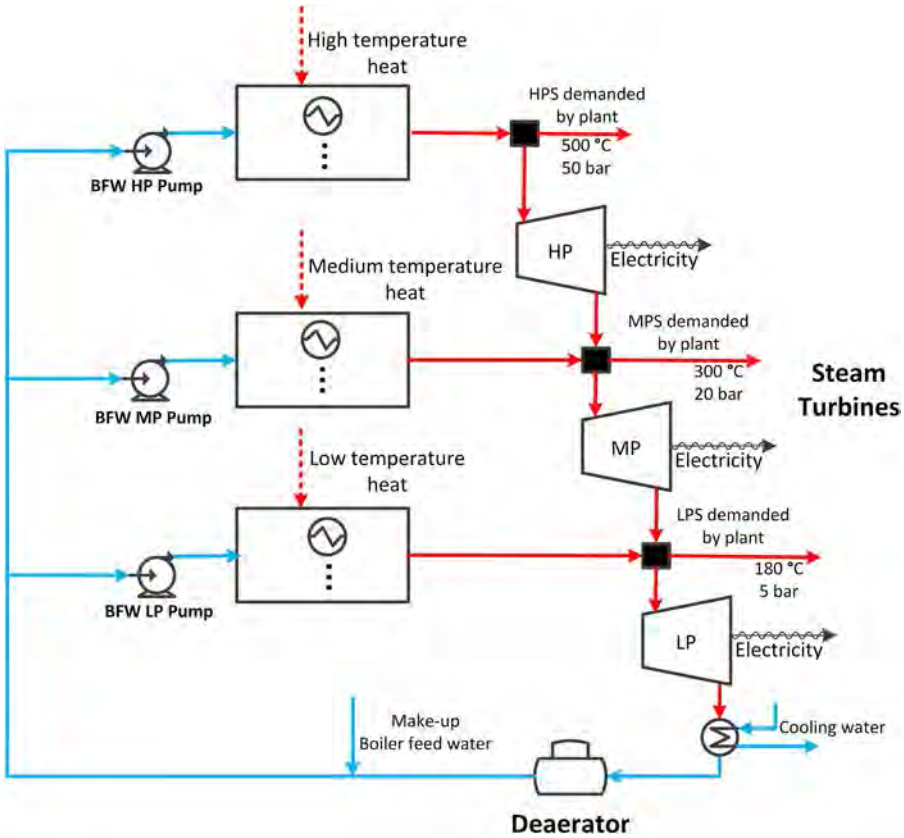

Figure 14. The model for the HRSG section of the plant.

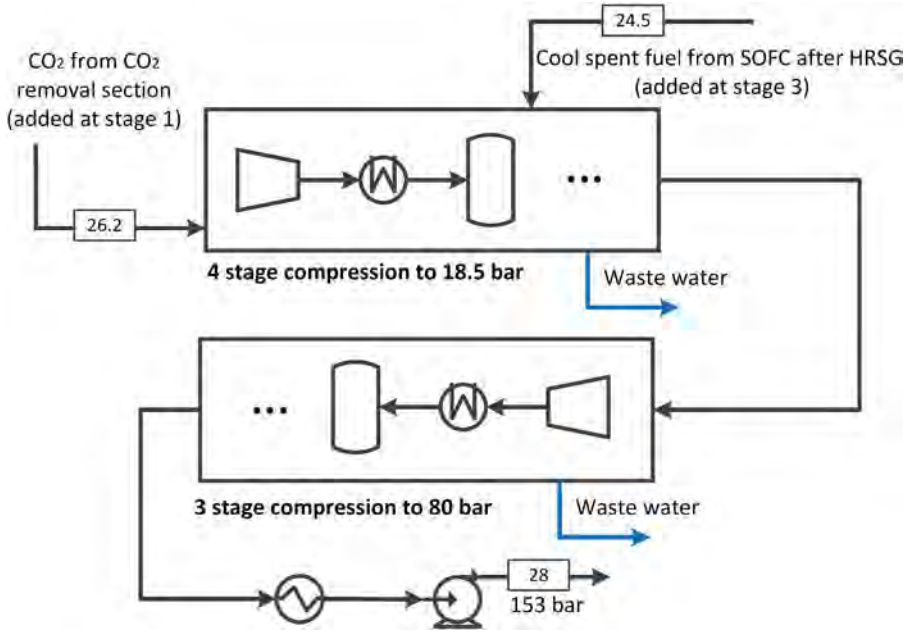

Figure 15. CO_2 compression section.

electricity, gas-turbine-generated electricity, FT liquids, methanol, and DME). Stream numbers in Table 4 correspond to the stream labels in Figures 2–16. In addition, a summary of key energy balance results is provided in Table 5. The thermal efficiency, as reported in Table 5, is defined as follows:

$$\textit{Thermal Efficiency}(HHV) = \frac{HHV_{DME} + HHV_{MeOH} + HHV_{Diesel} + HHV_{gasoline} + W_{elec}}{HHV_{biomass} + HHV_{naturalgas} + Q_{nuclearheat}}$$

where W_{elec} is the net electric work (AC, grid quality) generated by the plant, $Q_{nuclearheat}$ is the amount of heat collected from the nuclear reactor for CuCl process purposes (not the energy content of the uranium), and the *HHV* terms are the higher heating values of the fuels produced (DME, methanol, FT diesel, and FT gasoline) and feedstocks as appropriate. The relative amount of electricity produced is also on an HHV basis and is defined as follows:

$$\textit{Percentage of Output as Electricity} = \frac{W_{elec}}{W_{elec} + HHV_{DME} + HHV_{MeOH} + HHV_{Diesel} + HHV_{gasoline}}$$

The total direct GHG emissions reported in Table 5 are expressed in CO_2 emissions equivalents (CO_2e) using the standard International Panel on Climate Change 100-year metric.[39] They include only the GHG emissions directly leaving the plant through plant exhaust, which are primarily CO_2 with trace amounts of CH_4. This includes the effects of creating all utilities necessary since they are included in the model (e.g. various steam pressures, electricity, cooling services). It does not take into account upstream and downstream GHG emissions associated with production, use, transportation, or storage of CO_2, which is instead discussed in Part II of this work in detail.

The results of Table 5 show that Case 1.2, which uses classic steam generation in the RSC, has a lower thermal efficiency by about 2 percentage points than using the integrated reformer, all else being equal. The power and work breakdown for these two cases is shown in Table 6. More power is produced in the high and medium pressure turbines in the HRSG in Case 1.2 because of the extra steam generation, and the total electric power produced in Case 1.2 as a percentage of the total energy output is also about 1 percentage point higher. However, the overall efficiency of Case 1.1 is higher because the additional liquid fuels that can be produced from the integrated reforming process more than makes up for this difference. This is expected because Case 1.1 makes better use of the exergy available in the RSC by making more liquid fuels instead of high pressure steam.

Note that it is not possible to make conclusions as to whether one design concept is better than the other in general, because these base cases have not been optimized, nor have we defined economic or processing objectives. That will be explored in detail in a future work.

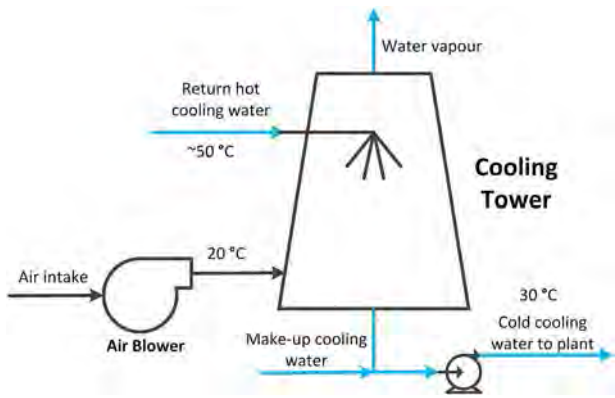

Figure 16. The model of the cooling tower section.

Table 4. Selected stream conditions for base case 1.1 * Wood has a mass flow rate of 100 t/h

Stream ID	1	2	3	4	5	5.1	6.1	6.2	7	8	9
T (°C)	16	500	30	168	300	350	500	500	31	806	200
P (MPa)	0.11	5.0	4.6	4.7	3.48	3.44	5.0	5.0	4.5	2.38	4.33
F (kmol/h)	*	161	273	1522	677	1062	356	2002	5726	4168	9365
Vapour Fractions	Solid	1	1	1	1	1	1	1	0	1	1
Mole Fractions (% unless otherwise noted)											
Wood	*										
H_2						1.8				43	17.7
CO						61 ppm				10.4	31.8
CO_2			100		1	2				3.3	10.6
H_2O		100				30.7	100	100	100	39.8	39.6
Ar				0.3							518 ppm
O_2				99.5							
N_2				0.2	0.8	0.5				0.1	0.2
NH_3											8 ppm
H_2S											14 ppm
HCl											576 ppm
CH_4					93.9	64.9				3.3	60 ppm
C_2H_6					3.2						
C_3H_8					0.7						
C_4H_{10}					0.4						

Stream ID	12	13	14	15	16	20	20.1	21	22	22.1	22.2
T (°C)	40	40	40	40	40	40	500	100	30	500	102
P (MPa)	2.26	2.26	4.3	4.3	4.3	4.3	5.0	4.14	3.0	5.0	2.95
F (kmol/h)	4168	2515	9365	3693	5672	1506	405	1911	2657	1395	1419
Vapour Fractions	0.6	1	0.61	0	1	1	1	1	1	1	1
Mole Fractions (% unless otherwise noted)											
H_2	43	71.2	17.7	5 ppm	29.2	29.2		43			
CO	10.4	17.3	31.8	3 ppm	52.6	52.6		21.4			
CO_2	3.3	5.5	10.6	102 ppm	17.5	17.5		33.8	1		
H_2O	39.8	0.3	39.6	100	0.2	0.2	100	1.3		100	
Ar			518 ppm	90 ppb	855 ppm	855 ppm		674 ppm			0.3
O_2											99.5
N_2	0.1	0.2	0.2	16 ppb	0.3	0.3		0.3	0.8		0.2
NH_3			8 ppm	18 ppm	989 ppb	989 ppb		779 ppb			
H_2S			14 ppm	365 ppb	23 ppm	23 ppm		18 ppm			
HCl			576 ppm	9 ppm	945 ppm	945 ppm		745 ppm			
CH_4	3.3	5.5	60 ppm	5 ppb	99 ppm	99 ppm		78 ppm	93.9		
C_2H_6									3.2		
C_3H_8									0.7		
C_4H_{10}									0.4		

Stream ID	22.3	23	24	24.1	24.2	24.3	24.4	24.5	24.6	25
T (°C)	500	40	80	15	15	700	476	1346	39	104
P (MPa)	5.0	2.77	2.76	0.1	0.1	0.1	0.11	1.76	2.1	5.2
F (kmol/h)	3813	8733	4020	12299	6308	8944	10160	7061	6675	10348
Vapour Fractions	1	1	1	1	1	1	1	1	1	1
Mole Fractions (% unless otherwise noted)										
H_2		67.5	62			80 ppm		721 ppm	50.3	56
CO		20.9	25.3			312 ppm		350 ppm	24.4	27.8
CO_2		10	10.4	300 ppm	300 ppm	9.1	363 ppm	46.1	21.6	14.3
H_2O	100	0.3	0.3	1.1	1.1	11.2	1.3	52.9	0.1	0.4
Ar		519 ppm	475 ppm	0.9	0.9	0.7	1.1	0.2	0.1	541 ppm
O_2				20.8	20.8	6.7	4	0.1		
N_2		0.3	0.3	77.2	77.2	72.2	93.4	0.6	0.6	0.3
H_2S			4 ppm					12 ppm	12 ppm	9 ppm
HCl			152 ppm			93 ppm	328 ppm		500 ppm	344 ppm
CH_4		1	1.7					231 ppm	2.4	1.2
SO_2						2 ppm				
CH_3OH								7 ppm	0.4	
C_2H_5OH								22 ppb	2 ppm	
$HCOOCH_3$								2 ppm	207 ppm	

Stream ID	25.1	25.2	25.3	26	26.1	26.2	26.3	27	27.1	27.2
T (°C)	29	40	30	73	20	48	46	50	43	89
P (MPa)	5.04	0.1	0.68	4.0	1.0	0.16	4.17	4.09	3.98	0.28
F (kmol/h)	2413	230	890	3449	293	578	36	4870	2204	31
Vapour Fractions	0	0	0	1	1	0.99	0	1	1	0
Mole Fractions (% unless otherwise noted)										
H_2	0.3			56	100	0.6		62	56.8	360 ppm
CO	0.3			27.8		0.2		30.8	23.9	417 ppm
CO_2	7.1			14.3		92.4		2.7	6.5	0.4
H_2O	6.9	62 ppm	2 ppb	0.4		6.7	100	0.2	616 ppm	
Ar	26 ppm			541 ppm		34 ppm		0.3	0.8	28 ppm
O_2										
N_2	80 ppm			0.3		77 ppm		1.3	2.9	47 ppm
H_2S	13 ppm			9 ppm		50 ppm		106 ppb	232 ppb	72 ppb
HCl	616 ppm			344 ppm						
CH_4	971 ppm			1.2		719 ppm		2.6	7.9	637 ppm
SO_2										
CH_3OH	85	99.6	0.5							
C_2H_5OH	0.1	0.4	166 ppb							
$HCOOCH_3$	632 ppm	206 ppb	479 ppb							
DME			99.5							
C_2 to C_5									1.1	4.7
C_6 to C_{11}									0.1	94.3
C_{12} to C_{20}									300 ppb	43 ppm

Stream ID	27-3	28
T (°C)	200	57
P (MPa)	0.3	15.3
F (kmol/h)	41	3847
Vapour Fractions	0	0
Mole Fractions (% unless otherwise noted)		
H_2		0.2
CO		995 ppm
CO_2	1 ppb	98.1
H_2O		7 ppm
Ar		0.3
O_2		0.2
N_2		1.1
H_2S		29 ppm
CH_4		532 ppm
CH_3OH		572 ppb
C_2H_5OH		3 ppb
$HCOOCH_3$		1 ppm
C_2 to C_5	496 ppb	
C_6 to C_{11}	3.4	
C_{12} to C_{20}	90.8	

The largest consumers of power are the ASU, biomass crushing, and air compression for the power generation units, together comprising more than 77 % of the parasitic load. Most of the remaining units are relatively small. The power surplus indicates that a greater percentage of syngas could be used for liquid fuels if desired and still have enough energy available to meet all process electricity and steam needs.

The contribution of the nuclear component is relatively small at roughly 8–9 % of the total energy input. This indicates that the need for hydrogen required for syngas upgrading for fuel production is relatively small. Although the nuclear component could increase in importance as more liquid fuels are produced, about 75 % of the output is already liquid fuels in this example and so the nuclear hydrogen demand would not increase by more than roughly a third. In order to increase the potential contribution of the nuclear component, it may be beneficial to use additional nuclear heat for steam methane reforming in the ATR (if present) and/or instead of using the IR, as proposed by Khojestah Salkuyeh and Adams.[14]

The GHG emissions reductions potential using CCS is quite large, with about 80 % of the CO_2 produced captured in this example. For the CCS-enabled plants, the atmospheric emissions primarily come through gas turbine exhaust, since post-combustion capture is not considered due to its relative inefficiency.[40] If only SOFCs were used, then the GHG emissions arising from power generation could approach trivially small amounts, since even the off-gases from liquid production can be used in the SOFC. In case 1.1, approximately 45 t/h of carbon (atomic) enters the process via wood, and about

Table 5. Summary of mass and energy balance results for the two base case examples, assuming 365/24/7 operation at 100 % capacity

Case	1.1	1.2
Uses CCS?	Yes	Yes
Syngas cooling	IR	RSC
Energy Inputs (MW by HHV)		
Wood chips	550	550
Natural gas	833	664
Nuclear heat	117	117
Total	1500	1331
Energy Outputs (MW by HHV or electricity)		
Electricity	170	152
Diesel	103	86
Gasoline	46	39
Methanol	47	39
DME	360	303
Total	726	619
Thermal Efficiency (%HHV)	48.4 %	46.5 %
Carbon efficiency (C in Products/C in Feedstock)	39.1 %	36.7 %
Direct GHG emissions (tCO_2e/yr)	314 074	295 253
Captured CO_2 (tCO_2e/yr)	1 236 501	1 171 601
Direct CO_2 emissions per MJ_{HHV} products (kg/MJ_{HHV})	9.96	9.36

42 t/h of carbon enters via natural gas. Of this, about 34 t/h of C is recovered as a fuel product. This gives a carbon efficiency of approximately 39.1 %, which is defined as the percentage of carbon in the feed that ends up in a useful product (instead of captured or emitted CO_2 or other GHGs). This is quite good considering that more than half of the carbon source is biogenic, although a detailed life cycle analysis is left for future work. Case 1.2 has a lower carbon efficiency because it has a lower percentage of liquid fuels produced. For the same reason, Case 1.2 has lower direct CO_2 emissions per MJ of products produced,

Table 6. Summary of power consumed or produced by unit for the two cases, in MW

	Case	Case		Case	Case
Biomass Gasification	**1.1**	**1.2**	*Cooling Towers*	**1.1**	**1.2**
Biomass crushing	11.0	11.0	Air compressors	3.5	3.2
ASU	41.3	37.9	Water pump	8.3	7.6
Primary O_2 booster (to 1.29 MPa)	0.3	0.3	*Power Island*		
Secondary O_2 booster (to 4.7 MPa)	2.0	2.0	Gas turbine air compression	26.5	21.7
Quench water pump	0.2	0.2	Gas turbine power production	−67.1	−55.3
Syngas Mixing and Upgrading			SOFC cathode air compression.	47.8	41.6
O_2 boost compression (to 3.0 MPa)	1.0	1.0	FT off-gas expander	−0.1	−0.1
Syngas compressor (from IR)	1.4	N/A	MeOH off-gas expander	−0.1	−0.1
Syngas compressor (from ATR)	2.2	2.2	Syngas expander for SOFC anode	−0.7	−0.6
Syngas compressor (MeOH-bound)	2.8	2.5	SOFC stack power	−151.4	−131.2
CO_2 Capture Sections			O_2 boost compressor	0.3	0.2
MDEA Section	0.3	0.3	Cathode exhaust turbine stage 1	−29.2	−25.4
FT of-gas recycle compressor	0.2	0.2	Cathode exhaust turbine stage 2	−19.8	−17.2
CO_2 Compression Section			*Heat Recovery and Steam Generation*		
Compression train 1 (to 1.9 MPa)	4.8	4.6	Boiler feedwater pumping	0.7	0.7
Compression train 2 (to 8.0 MPa)	4.5	4.2	High pressure gas turbine	−2.7	−5.4
Supercritical pumping to pipeline	0.9	0.9	Medium pressure gas turbine	−13.9	−15.3
FT Synthesis Section			Low pressure gas turbine	−48.2	−46.3
O_2 boost compressor (to 4.0 MPa)	0.3	0.2			
Distillation bottoms pump	0.0	0.0	**GROSS POWER CONSUMPTION**	**163**	**145**
Flash drum vapor product compr.	0.4	0.3	**GROSS POWER PRODUCTION**	**333**	**297**
Distillate off gas recycle compr.	1.0	0.8	**NET POWER PRODUCTION**	**170**	**152**
Methanol Synthesis Section					
Off-gas recycle compressor	1.1	1.0			
Methanol pump	0.2	0.1			

since CO_2 capture happens mostly as a result of power production as opposed to liquid fuel production. Neither metric indicates that Case 1.2 is any more or less environmentally friendly than Case 1.1, because the product portfolios are different. That will be determined in a future work by considering a complete life cycle analysis of optimized processes for specific business objectives.

Uncertainty

As with any model, the results shown in the previous section are based on the various assumptions used when developing the model, and thus there are uncertainties in the results based on these assumptions. For example, variations in the proximate or ultimate analysis characteristics of the biomass used would have cascading impacts on the simulation results of virtually every unit operation model downstream. Changes to other parameters such as compressor efficiencies, catalyst properties, operating temperature ranges, and physical property model parameters also would have an impact on key performance metrics, such as energy efficiency, carbon efficiencies, carbon dioxide emissions, or product yields. In addition, the use of the two ROSSMs introduces small mass balance errors, since they do not include mass balance closure by design as a trade-off for avoiding the use of very rigorous models. However, the model presented in this work is still very useful in that it can be used to explore the effects of changes in these parameters quite quickly, and that meaningful conclusions can be made when comparing different processes to each other when using a consistent set of assumptions.

The selection of the best product designs, such as which feedstocks and design approaches to use, is particularly sensitive to the market prices of the feedstocks and products. For example, prior work on coal-gas-and-nuclear-to-liquid systems found that the assumed average lifetime market prices of the feedstocks and products (over a 30 year period) has a strong impact on the optimal plant design.[14] In fact, the study found that the historical variability in the market between 2008 and 2012 was significant enough such that there could be no clear decision going forward as to whether the optimal design should use nuclear energy or not, should use natural gas or not, use carbon capture and sequestration or not, or use certain other design decisions such as how off-gases are recycled. In other words, depending on the market prices used to estimate the net present value of the process going forward over the lifetime of the plant, the optimal design changed significantly. A later review paper found that such observations were common in the literature for polygeneration applications, as their lifespans are typically 25 years or more.[17] Therefore, Part II of this work will include an uncertainty analysis similar those used in the previous studies to quantify the potential impact of these uncertainties on the underlying economics of the BGNTL concept. Those results will then be used to make decisions about the economic feasibility of the BGNTL concept as a whole under this uncertainty.

CONCLUSIONS

Two new biomass, gas, and nuclear-to-liquids polygeneration process superstructures were presented in this work, each using different levels of advanced technologies. The nuclear component is primarily integrated through syngas upgrading using hydrogen produced via the CuCl cycle, and is particularly suitable for next generation Canadian nuclear reactor designs, such as the CanDU SCWR. Ontario-grown cedar wood chips are used as one of the key feedstocks in conjunction with conventional pipeline natural gas. The process models have been provided as supplementary material on the repository at PSEcommunity.org so that they can be used by others for planning and design purposes.

The proposed superstructures are suitable for the co-production of electricity and various liquid fuels, and can be modified to suit whatever product portfolio is of most interest to the end user. Although there are various strengths and weaknesses to each of the different process types, the key difference is that the integrated reforming strategy uses the available heat of the RSC to make a larger percentage of higher value products (liquid fuels) than electricity, as compared to a classic steam generation strategy. However, the key differences in value between the processes are expected to be rooted in their environmental and economic properties, which are highly dependent on market conditions, public policy, and upstream and downstream end use supply chains. These issues are addressed in Part II of this work, which will use an optimization-based analysis that factors in capital and operating cost estimates, profitability analyses, cradle-to-grave life cycle analyses, and carbon taxes to make conclusions about which process designs are best suited for Ontario in different market conditions. The comparison of these designs to similar designs that do not use nuclear energy (and use a greater proportion of biomass instead) is also a subject of future work.

ACKNOWLEDGEMENTS

This work was funded by contributions from an NSERC Canadian Graduate Scholarship, an Ontario Graduate Scholarship, and an Ontario Early Researcher Award (ER13-09-213).

ABBREVIATIONS

ASU	air separation unit
ATR	autothermal reforming
BGNTL	biomass-gas-and-nuclear-to-liquids
BGTL	biomass-and-gas-to-liquids
CanDU	Canadian deuterium-uranium
CCS	carbon capture and sequestration
CO_2e	carbon dioxide emissions equivalents
DME	dimethyl ether
FT	Fischer-Tropsch
GHG	greenhouse gas
GT	gas turbine
HHV	higher heating value
HPS	high pressure steam
HRSG	heat recovery and steam generation
IR	integrated reformer
MDEA	methyldiethanolamine
MeOH	methanol
RSC	radiant syngas cooler
SCWR	supercritical water reactor
SMR	steam methane reformer / steam methane reforming
SOFC	solid oxide fuel cell
t	(metric) tonne = 1000 kg
WGS	water gas shift

APPENDIX

Table A1. ROSSM parameters for the integrated reformer model described in Equation (1) in the section called Biomass Processing and Gasification Section. The maximum absolute error is defined as the point with the highest difference between the predicted and actual values of Z_i divided by the actual value, for the 80 points explored. The model is only valid within the range of $506.9 \leq F_{NG} \leq 753.5(MW)$ and $2.6 \leq R_{S:C} \leq 4.0$, with $\bar{F_{NG}} = 637.329\ MW$ and $\bar{R_{S:C}} = 3.293$

Model Variable (i)	Z_1	Z_2	Z_3	Z_4	Z_5
Description	Required radiant cooling duty	CH_4 conversion	H_2O conversion	Tube side exit Temperature	Tube side pressure drop
Units Z_i of (and $a_{j,i}$)	MW	*unitless*	*unitless*	°K	MPa
$a_{1,i}$	5.726	1.068	0.864	1512	−1.4815
$a_{2,i}$	32.529	−0.679	−0.231	−362.9	2.106
$a_{3,i}$	10.417	0.257	−0.571	−86.65	1.768
$a_{4,i}$	−9.871	0.144	0.027	110.4	−0.7113
$a_{5,i}$	−2.601	−0.062	0.145	28.44	−0.4098
$a_{6,i}$	2.336	0.030	0.096	−72.49	−1.806
R^2 of training data	1.00	1.00	1.00	1.00	1.00
R^2 of testing data	1.00	0.99	1.00	1.00	0.998
Max abs error	0.04 %	0.14 %	0.15 %	0.03 %	0.01 %

Table A2. ROSSM model for the syngas CO_2 removal section described in the Carbon Dioxide Removal from Syngas section. The model is only valid within the range of $620.6025 \leq F_{CO2} \leq 1033.75$ (kmol/h) where F_{CO2} is the inlet flow rates of the CO_2 contained within the syngas feed for a syngas feed typical of FT synthesis applications and scales, with the normalization factors of $\bar{F_{CO2}} = 827.47$ kmol/h. The model has the form: $Z_i = a_{1,i} + a_{2,i}\frac{F_{CO2}}{\bar{F_{CO2}}}$

Model Variable (i)	Z_1	Z_2	Z_3	Z_4	Z_5	Z_6	Z_7
Description	MDEA makeup	H_2O makeup	Pump power	Reboiler duty	Condenser duty	Distillate cooler	Amine cooler
Units Z_i of (and $a_{j,i}$)	kmol/h	kmol/h	kW	kW	kW	kW	kW
$a_{1,i}$	5.595×10^{-4}	−1.235	3.099	−117.9	0.581	14.64	−74.48
$a_{2,i}$	6.709×10^{-3}	40.92	425	15 950	128.9	3220	7040
R^2 of training data	0.843	0.963	1	1	1	1	1
R^2 of testing data	0.812	0.900	0.997	0.998	0.999	0.999	0.991
Max abs error	5.0 %	5.0 %	0.7 %	0.6 %	0.4 %	0.4 %	1.1 %

REFERENCES

[1] Government of Ontario, *Ontario's Five Year Climate Change Action Plan 2016–2020* (p. 86), PIBS 9942, Government of Ontario, Toronto **2016**, http://www.applications.ene.gov.on.ca/ccap/products/CCAP_ENGLISH.pdf.

[2] Ontario Ministry of Energy, "Ontario's Long Term Energy Plan," *Government of Ontario*, **2013**, accessed on 20 August 2017, https://www.ontario.ca/page/ontarios-long-term-energy-plan.

[3] Environment and Climate Change Canada, "Pan-Canadian Approach to Pricing Carbon Pollution," **2016**, accessed 20 August 2017, https://www.canada.ca/en/environment-climate-change/news/2016/10/canadian-approach-pricing-carbon-pollution.html.

[4] Environment and Climate Change Canada, "Technical paper: federal carbon pricing backstop," *Government of Canada*, **2017**, accessed on 20 August 2017, https://www.canada.ca/en/services/environment/weather/climatechange/technical-paper-federal-carbon-pricing-backstop.html.

[5] Ontario Energy Board, "Ontario's System-Wide Electricity Mix: 2016 Data," *Ontario Energy Board*, **2017**, accessed on 20 August 2017, https://www.oeb.ca/sites/default/files/2016_Supply_Mix_Data.pdf.

[6] Environmental Commissioner of Ontario, "Facing Climate Change: Greenhouse Gas Progress Report, Chapter 2: Ontario's Carbon Footprint—Where are we now?," *Environmental Commissioner of Ontario*, **2016**, accessed on 20 August 2017, https://eco.on.ca/reports/2016-facing-climate- change/.

[7] D. B. Levin, H. Zhu, H. M. Beland, N. Cicek, B. E. Holbein, *Bioresource Technol.* **2007**, *98*, 654.

[8] S. Krigstin, S. Wetzel, W. Mabee, S. Stadnyk, *Forest Chron.* **2016**, *92*, 189.

[9] R. Levin, S. Krigstin, S. Wetzel, *Forest Chron.* **2011**, *87*, 33.

[10] World Nuclear Association, "Uranium in Canada," *World Nuclear Association*, **2017**, accessed on September 5, 2017, http://www.world-nuclear.org/information-library/country-profiles/countries-a-f/canada-uranium.aspx.

[11] M. Naidin, S. Mokry, F. Baig, Y. Gospodinov, Y. Zirn, I. Pioro, G. Naterer, *J. Eng. Gas Turb. Power* **2009**, *131*, 12901.

[12] G. F. Naterer, I. Dincer, C. Zamifirescu, *Hydrogen Production from Nuclear Energy*, Springer, London **2013**.

[13] L. Hosenzade, T. A. Adams II, *Int. J. Hydrogen Energ.* **2017**, *42*, 25048Y.

[14] Y. Khojestah Salkuyeh, T. A. Adams II, *Energ. Convers. Manage.* **2013**, *74*, 492.

[15] Y. Khojestah Salkuyeh, T. A. Adams II, *Energ. Convers. Manage*. **2014**, *88*, 411.

[16] T. A. Adams II, P. I. Barton, *Fuel Process. Technol*. **2011**, *92*, 639.

[17] T. A. Adams II, J. H. Ghouse, *Curr. Opin. Chem. Eng*. **2015**, *10*, 87.

[18] J. H. Ghouse, D. Seepersad, T. A. Adams II, *Fuel Process. Technol*. **2015**, *138*, 378.

[19] T. A. Adams II, P. I. Barton, *AIChE J*. **2010**, *56*, 3120.

[20] D. Hewson, A. Oo, K. J. Albion, A. Keir, *Biomass residuals study for OPG repowering program*, BM22, The University of Western Ontario Research & Development Park, Sarnia **2011**, http://www.canadiancleanpowercoalition.com/pdf/BM22%20-%20Biomass%20Residuals%20Study%20for%20OPG%20Repowering%20Program.pdf.

[21] L. Zhang, Y. Ninomiya, Q. Wang, T. Yamashita, *Fuel* **2011**, *90*, 77.

[22] A. Van der Drift, A. Boerrigter, H. Coda, B. Cieplik, M. K. Hemmes, K. Van Ree, H. J. Veringa, *Entrained flow gasification of biomass*, ECN-C–04-0.39 Revision A, Energieonderzoek Centrum Nederland, Amsterdam **2004**, https://www.ecn.nl/docs/library/report/2004/c04039.pdf.

[23] R. P. Field, R. Brasington, *Ind. Eng. Chem. Res*. **2011**, *50*, 11306.

[24] L. R. Clausen, B. Elmegaard, N. Houbak, *Energy* **2010**, *35*, 4831.

[25] J. H. Ghouse, T. A. Adams II, *Int. J. Hydrogen Energ*. **2013**, *38*, 9984.

[26] T. A. Adams II, P. I. Barton, *J. Power Sources* **2010**, *195*, 1971.

[27] T. A. Adams II, Y. Salkuyeh Khojestah, J. Nease, "Process and Simulations for Solvent-Based CO_2 Capture and Syngas Cleanup," *Reactor and Process Design In Sustainable Energy Technology*, F. Shi, Ed., Elsevier, Amsterdam **2014**, pp. 163–231.

[28] T. A. Adams II, P. I. Barton, *Int. J. Hydrogen Energ*. **2009**, *34*, 8877.

[29] M. S. Ferrandon, M. A. Lewis, D. F. Tatterson, R. V. Nankanic, M. Kumarc, L. W. Wedgewood, C. Nische, *Proceedings of the NHA Annual Hydrogen Conference* **2008**, *10*, 3310.

[30] G. F. Naterer, S. Suppia, L. Stolberg, M. Lewis, M. Ferrandon, Z. Wang, J. Avsec, *Int. J. Hydrogen Energ*. **2011**, *36*, 15486.

[31] Z. L. Wang, G. F. Naterer, K. S. Gabriel, R. Gravelsins, V. N. Daggupati, *Int. J. Hydrogen Energ*. **2010**, *35*, 4820.

[32] M. A. Rosen, *Energy* **2010**, *35*, 1068.

[33] P. V. Tsvetkov, *Nuclear Power Deployment, Operation, and Sustainability*, In Tech, Rijeka, Croatia **2010**.

[34] C. N. Hamelinck, A. P. C. Faaij, H. den Uil, H. Boerrigter, *Energy* **2004**, *9*, 1743.

[35] K. V. Bussche, G. H. Froment, *J. Catal*. **1996**, *161*, 1.

[36] G. Bercic, J. Levec, *Ind. Eng. Chem. Res*. **1993**, *32*, 2478.

[37] W. D. Seider, J. D. Seader, D. R. Lewin, S. Widago, *Product and Process Design Principles: Synthesis, Analysis and Design*, 3rd edition, Wiley, Hoboken, NJ **2008**.

[38] J. A. Queiroz, V. M. S. Rodrigues, H. A. Matos, F. G. Martins, *Energ. Convers. Manage*. **2012**, *64*, 43.

[39] G. Myhre, D. Shindell, F.-M. Bréon, W. Collins, J. Fuglestvedt, J. Huang, D. Koch, J.-F. Lamarque, D. Lee, B. Mendoza, T. Nakajima, A. Robock, G. Stephens, T. Takemura, H. Zha, 13: Anthropogenic and Natural Radiative Forcing, *Climate Change 2013: The Physical Science Basis, Contribution of Working Group I to the Fifth Assessment Report of the Intergovernmental Panel on Climate Change*, T. F. Stocker, D. Qin, G.-K. Plattner, M. Tignor, K. S. Allen, J. Boschung, A. Nauels, Y. Xia, V. Bex, P. M. Midgley, Eds., Cambridge University Press, Cambridge **2013**, p. 731.

[40] T. A. Adams II, L. Hoseinzade, P. B. Madabhushi, I. J. Okeke, *Processes* **2017**, *5*, 44.

[41] M. A. Rosen, J. D. Scott. *Int. J. Hydrogen Energ*. **1998**, *23*, 6539.

Manuscript received January 16, 2018; revised manuscript received April 10, 2018; accepted for publication April 10, 2018.